2024 American Control Conference (ACC)
July 8-12, 2024. Toronto, Canada

State-Space System Identification beyond the Nyquist Frequency with Collaborative Non-Uniform Sensing Data

Xiaohai Hu†, Thomas L. Chu†,and Xu Chen†,⋆

***Abstract*— In a multirate sampled-data system encompassing a continuous-time process and multiple output samplers with periods n_1T and n_2T, coupled with a zero-order hold with a period of mT for the input, we introduce an innovative approach that leverages non-uniform data collated through a coprime collaborative sensing mechanism. The ultimate aim is to identify the intricate dynamics governing the system. The predominant challenge – relating to the accurate identification and representation of the multirate system dynamics – is addressed by pioneering a lifted state-space model for the system. This model is achieved by building upon and extending the subspace system identification. Moving forth, using this elevated model as a foundational basis, we seamlessly extract the single-rate system through an eigenvalue decomposition process. The proposed methodology's efficacy is empirically tested through demonstrative examples with multiple orders and varying coefficients.**

I. Introduction

Multirate systems play a pivotal role in diverse areas such as process control within chemical reactions [1], auditory aids in human audio and speech processing [2], [3], aerospace industry [4] and addictive manufacturing [5]–[7]. For example, polymerization reactors [8] often employ a gas chromatography to keep track of reactant concentrations. The measured sampling rate of these concentrations tends to be slower than other parameters such as temperature or pressure. Despite this, modifications to the reactor's input can be made quickly. This rate difference defines a multirate system mode, where the characteristic trait is typically a slower sampled output compared to the input.

The standard configuration of a multirate system is to have the output and input sampled at two different rates. The adoption of non-uniform sampling will bring forth a plethora of advantages. It allows for richer sampling in areas of significant interest, proving invaluable in regions marked by pronounced variability or intricacy. Additionally, non-uniform sampling promotes the use of computational resources by focusing on fewer samples in regions that are more predictable or stable. Furthermore, it offers the flexibility to align with the inherent characteristics of the data, which can pave the way for more refined models or representations. On the flip side, non-uniform sampling serves as a bulwark against the adverse impacts of aliasing, particularly when the mean sampling rate falls short of twice the desired Nyquist sampling frequency. Therefore, it is imperative to acknowledge the complexities introduced by non-uniform sampling, especially regarding system identification algorithms. The challenges associated with procuring analytical solutions have cast a shadow of uncertainty over the practicality of non-uniform data.

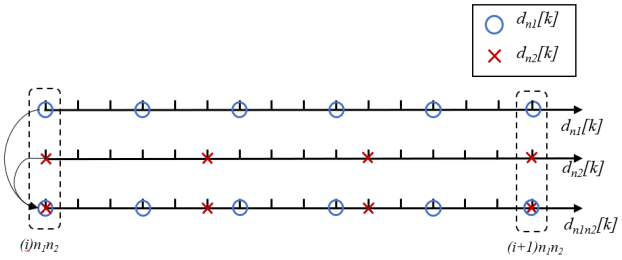

Fig. 1. Irregular and sparse measurements from two sensors with different sampling rates, i.e., $n_1 = 3$ and $n_2 = 5$. Parameter estimation is relevant only at times that are integer multiples of $n_1 \times n_2$. [14]

Historically, multirate system identification has been a subject of rigorous research since Kranc's seminal contribution in 1957 [9]. Three predominant techniques have been employed: the lifting technique for state-space model identification [10], polynomial transformation [11], and the stochastic gradient method [12], [13]. This paper introduces a novel concept of system identification with complete coprime collaborative sensing. The proposed approach employs two slow sensors with distinct sampling rates, synchronized and processed to identify system dynamics surpassing the individual sensor's capabilities, as illustrated in Fig. 1. This collaborative methodology retains each sensor's uniform sampling rate while enhancing overall data resolution. We attain the identification goal by first formulating a lifted multirate system (Section II), developing a modified subspace system identification to discern the state space of the lifted model (Section III), and then recovering the original fast-rate model via an eigenvalue analysis (Section IV). The efficacy of the proposed approach is validated in the concluding sections through case studies on partially randomly selected system models and a comparison among different sensors.

II. Problem Formulation

We consider the problem of system identification for a multirate system as shown in Fig. 2. This system consists of a continuous-time plant, $P(s)$, which receives an input signal, $u[n]$, through a zero-order hold H_{mT} operating at a period of mT, ensuring the continuous nature of the signal. The output

† X. Hu, T. L. Chu, and X. Chen are with the Mechanical Engineering Department, University of Washington, Seattle, WA 98195, USA. {hxh,tchu,chx}@uw.edu. ⋆: corresponding author.

This material is based upon work supported by the National Science Foundation under Grants No. CMMI-1953155 and No. CMMI-2141293. The opinions, findings, and conclusions, or recommendations expressed are those of the author(s) and do not necessarily reflect the views of the National Science Foundation.

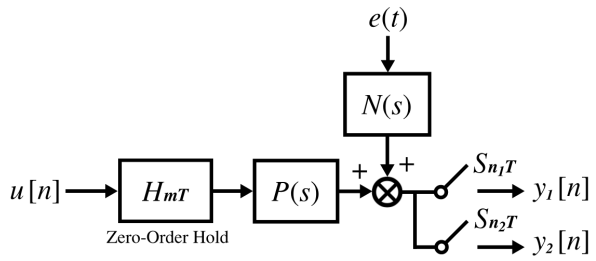

Fig. 2. A Multirate System with two samplers and noise, $e(t)$.

of the system is then sampled at different rates. In this paper, we specifically focus on the case where the system has two slow sensors. The two sensors sample at S_{n_1T} and S_{n_2T} with periods of n_1T and n_2T, respectively. For simplification, we also omit "s" in our subsequent derivations. We assume the following:

1) The input is sampled faster than the outputs, i.e., $m < n_i$ for all i, which is common in practice [1].
2) The values m, n_1, and n_2 are coprime with respect to each other. If m and any n_i are not coprime, the common factor can be extracted. For n_1 and n_2, coarrays of coprime arrays provide enhanced information, facilitating estimation with fewer sensor elements, as highlighted in [15].

A. Lifting Technique for Multi-rate Systems

To deal with the multirate systems, one has to address the challenge of different sampling rates in the input $u[k]$ and outputs $y_i[k]$'s. When only one sensor exists, such mismatched input and output can be addressed with the lifting technique [16], [17]. Here, we leverage the lifting technique to transform the multi-sensor multi-rate system into a single-rate system operating at a common multiple period, mn_1n_2T.

More specifically, we denote the lifting operator, $L_{n_1n_2}$, to map the input signal u to a vector input signal $\underline{u}$:

$$\{u(0),u(1),\ldots\}\mapsto\left\{\begin{pmatrix}u(0)\\u(1)\\\vdots\\u(n_1n_2-1)\end{pmatrix},\begin{pmatrix}u(n_1n_2)\\u(n_1n_2+1)\\\vdots\\u(2n_1n_2-1)\end{pmatrix},\ldots\right\} \tag{1}$$

or compactly denoted as $\underline{u}=L_{n_1n_2}u$.

The process of lifting is characterized by several distinct properties. Specifically, lifting is non-causal, norm-preserving, and invertible, i.e. $L^{-1}L=LL^{-1}=I$ [16], [17]. The lifting technique retains the data-rich input by packaging the vector of input as a set of equally sized vectors. The signals are uplifted to a lower sampling rate, often referred to as a common or mutual sampling period, which transforms the system from a multi-rate framework to a single-rate schema.

Fig. 3 shows the proposed model transformation where outputs from channel one, $y_1[k]$, and two, $y_2[k]$, are lifted by L_{mn_2} and L_{mn_1}, respectively, and the input is lifted by $L_{n_1n_2}$. As a result of these operations, the initial multi-rate system becomes a multiple-input, multiple-output (MIMO) lifted system, which operates singularly at a longer period of mn_1n_2T.

B. State-Space Equations for The Lifted Model

Consider the lifted system represented as $\underline{P}$, which maps $\underline{u}$ to $\underline{y_i}$ ($i\in\{1,2\}$). Let $\underline{P_1}$ and $\underline{P_2}$ be the lifted transfer functions of the plant, P, corresponding to channel one and two of the output sensors. Our objective here is to delineate the representation as derived from both channel one and two. Further elaboration will reveal that by combining the output information from multiple sensors, an analytical solution for the single-rate state space model can be acquired.

From Fig. 3, the representation for channel one is expressed as $\underline{P_1}=L_{n_2m}S_{n_1T}PH_{mT}L^{-1}_{n_1n_2}$. Building upon the proposition presented in [17], we can derive the state-space representation $\underline{P_1}$ as

$$\underline{P_1}(z)=\left[\begin{array}{c|c|c|c}A_{mT}^{n_1n_2}&A_{mT}^{n_1n_2-1}B_{mT}&\cdots&B_{mT}\\\hline C&D&\cdots&0\\CA^{n_1}&CA^{n_1-m}B_{mT}&\cdots&0\\\vdots&\vdots&\ddots&\vdots\\CA^{(n_2m-1)n_1}&CA^{mn_1n_2-n_1-m}B_{mT}&\cdots&0\end{array}\right] \tag{2}$$

Similarly, we can establish the state-space equations for $\underline{P_2}$. It is noteworthy that while the matrices, A and B, are identical for P_1 and P_2, the corresponding C and D matrices differ in dimensions. This observation confirms the understanding that varied sampling rates do not alter the state count. We then have the state-spaces system representations (for $i=1,2$):

$$P_i(z)=\left[\begin{array}{c|c}A_P&B_P\\\hline C_i&D_i\end{array}\right], \tag{3}$$

By vertically concatenating the C matrices, we obtain

$$P(z)=\left[\begin{array}{c|c}A_P&B_P\\\hline C_1&D_1\\C_2&D_2\end{array}\right]. \tag{4}$$

A detailed depiction is presented in Eq. (7). Given that the resulting output is $y=[\underline{y_1}^T\ \underline{y_2}^T]^T$, the state space is formulated as

$$x[k+1]=A_px[k]+B_p\underline{u}[k] \tag{5}$$

$$\begin{bmatrix}y_1(0)\\y_1(n_1T)\\\vdots\\y_1((n_2m-1)n_1T)\\-\\y_2(0)\\y_2(n_1T)\\\vdots\\y_2((n_1m-1)n_2T)\end{bmatrix}=\begin{bmatrix}C_1\\-\\C_2\end{bmatrix}x(k)+\begin{bmatrix}D_1\\-\\D_2\end{bmatrix}\begin{bmatrix}u(0)\\u(mT)\\\vdots\\u((n,n_2-1)mT)\end{bmatrix}. \tag{6}$$

where the output $\underline{y}$ is rich in data by using both sensors, containing n_2m+n_1m measurements.

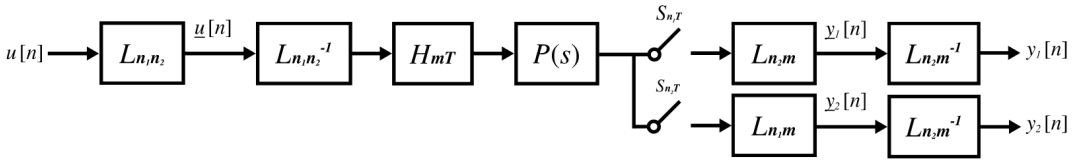

Fig. 3. Lifted Multirate System, where the input has a zero-order hold (mT) and output samples at periods n_1T and n_2T under collaborative sensing.

$$\left[\begin{array}{c|ccc} A^{mn_1n_2} & \left(\sum_{i=mn_1n_2-m}^{mn_1n_2-1} A^i\right)B & \left(\sum_{i=mn_1n_2-2m}^{mn_1n_2-m-1} A_i\right)B & \cdots & \left(\sum_{i=0}^{m-1} A^i\right)B \\ \hline C & D & 0 & \cdots & 0 \\ CA^{n_1} & C\left(\sum_{i=n_1-m}^{n_1-1} A^i\right)B & D + C\left(\sum_{i=0}^{n_1-m-1} A^i\right)B & \cdots & 0 \\ \vdots & \vdots & \vdots & & \vdots \\ CA^{(n_2m-1)n_1} & C\left(\sum_{i=mn_2-n_1-m}^{mn_2-n_1-1} A^i\right)B & C\left(\sum_{i=mn_2-n_1-2m}^{mn_2-n_1-m-1} A^i\right)B & \cdots & 0 \\ C & D & 0 & \cdots & 0 \\ CA^{n_2} & C\left(\sum_{i=n_2-m}^{n_2-1} A^i\right)B & D + C\left(\sum_{i=0}^{n_2-m-1} A^i\right)B & \cdots & 0 \\ \vdots & \vdots & \vdots & & \vdots \\ CA^{(n_1m-1)n_2} & C\left(\sum_{i=mn_1-n_2-m}^{mn_1-n_2-1} A^i\right)B & C\left(\sum_{i=mn_1-n_2-2m}^{mn_1-n_2-m-1} A^i\right)B & \cdots & 0 \end{array}\right] \tag{7}$$

III. Subspace System Identification of The Lifted Model

The proposed system transformation employs MIMO subspace system identification, initiating with the estimation of state vectors followed by the derivation of state-space realization.

A. Estimation of State Vectors

The lifted state-space model transforms the system into a MIMO system and is given by

$$\begin{aligned} \underline{x}[k+1] &= \underline{A}\,\underline{x}[k] + \underline{B}\,\underline{u}[k] \\ \underline{y}[k] &= \underline{C}\,\underline{x}[k] + \underline{D}\,\underline{u}[k] \end{aligned} \tag{8}$$

Given the input sequence $\{\underline{u}[0], \underline{u}[1], \ldots, \underline{u}[N-1]\}$ and output sequence $\{\underline{y}[0], \underline{y}[1], \ldots, \underline{y}[N-1]\}$, state order n, and time horizon K (where $K > n$), we form the input and output Hankel matrices as described in [18]:

$$U_{0|K-1} = \begin{bmatrix} \underline{u}[0] & \underline{u}[1] & \ldots & \underline{u}[N-1] \\ \underline{u}[1] & \underline{u}[2] & \ldots & \underline{u}[N] \\ \vdots & \vdots & \ddots & \vdots \\ \underline{u}[K-1] & \underline{u}[K] & \ldots & \underline{u}[K+N-2] \end{bmatrix}, \tag{9}$$

$$Y_{0|K-1} = \begin{bmatrix} \underline{y}[0] & \underline{y}[1] & \ldots & \underline{y}[N-1] \\ \underline{y}[1] & \underline{y}[2] & \ldots & \underline{y}[N] \\ \vdots & \vdots & \ddots & \vdots \\ \underline{y}[K-1] & \underline{y}[K] & \ldots & \underline{y}[K+N-2] \end{bmatrix}. \tag{10}$$

The dimensions of $U_{0|K-1}$ and $Y_{0|K-1}$ are Kn_1n_2N and $Km(n_1+n_2)N$, respectively. The row dimension arises from the interaction of the time horizon K with the number of inputs and outputs. After the lifting procedure, the input gets augmented by a factor of n_1n_2 and the output by m, with the column length designed to encompass the given data points.

By recursively using Eq. (8), the input-output relationship can be expressed as [19]

$$\begin{bmatrix} \underline{y}[k] \\ \underline{y}[k+1] \\ \vdots \\ \underline{y}[k+K-1] \end{bmatrix} = \begin{bmatrix} C \\ CA \\ \vdots \\ CA^{K-1} \end{bmatrix} \underline{x}[k] + \begin{bmatrix} D & 0 & \cdots & 0 \\ CB & D & \cdots & 0 \\ \vdots & \ddots & \ddots & \vdots \\ CA^{K-2}B & \cdots & CB & D \end{bmatrix} \begin{bmatrix} \underline{u}[k] \\ \underline{u}[k+1] \\ \vdots \\ \underline{u}[k+K-1] \end{bmatrix} \tag{11}$$

Here, the Extended Observability Matrix is defined as $\mathcal{O}_K = \begin{bmatrix} C & CA & \cdots & CA^{K-1} \end{bmatrix}^T$.

Let Ψ_K denote the Toeplitz matrix

$$\Psi_K = \begin{bmatrix} D & & & \\ CB & D & & \\ \vdots & \ddots & \ddots & \\ CA^{K-2}B & \cdots & CB & D \end{bmatrix}. \tag{12}$$

For notational convenience, we introduce the column vectors

$$\boldsymbol{u}_K[k] = \left[\underline{u}[k]^{\mathrm{T}}, \underline{u}[k+1]^{\mathrm{T}}, \ldots, \underline{u}[k+K-1]^{\mathrm{T}}\right]^{\mathrm{T}} \in \mathbb{R}^{Kn_1n_2}, \tag{13}$$

$$\boldsymbol{y}_K[k] = \left[\underline{y}[k]^{\mathrm{T}}, \underline{y}[k+1]^{\mathrm{T}}, \ldots, \underline{y}[k+K-1]^{\mathrm{T}}\right]^{\mathrm{T}} \in \mathbb{R}^{Km}. \tag{14}$$

The Hankel matrices, in terms of $\boldsymbol{u_K}[k]$ and $\boldsymbol{y_K}[k]$, are

$$U_{0|K-1} = \left[\boldsymbol{u}_K[0], \boldsymbol{u}_K[1], \ldots, \boldsymbol{u}_K[N-1]\right], \tag{15}$$

$$Y_{0|K-1} = \left[\boldsymbol{y}_K[0], \boldsymbol{y}_K[1], \ldots, \boldsymbol{y}_K[N-1]\right]. \tag{16}$$

Then, we have

$$\begin{bmatrix} U_{0|K-1} \\ Y_{0|K-1} \end{bmatrix} = \begin{bmatrix} I_{Km} & 0_{Km\times n} \\ \Psi_K & \mathcal{O}_K \end{bmatrix} \begin{bmatrix} U_{0|K-1} \\ X_0 \end{bmatrix} \tag{17}$$

where the past states (or initial states) $X_p = X_0 = [x[0], x[1], \cdots, x[N-1]] \in \mathbb{R}^{n\times N}$.

The future input and output are defined as

$$\begin{aligned} U_f &= U_{K|2K-1} \\ &= \begin{bmatrix} \boldsymbol{u}_K[K] & \boldsymbol{u}_K[K+1] & \cdots & \boldsymbol{u}_K[N+K-1] \end{bmatrix}, \\ Y_f &= Y_{K|2K-1} \\ &= \begin{bmatrix} \boldsymbol{y}_K[K] & \boldsymbol{y}_K[K+1] & \cdots & \boldsymbol{y}_K[N+K-1] \end{bmatrix}. \end{aligned} \tag{18}$$

By repeatedly using Eq. (8) similar to Eq. (17), we also have

$$Y_{K|2K-1} = \mathcal{O}_K X_K + \Psi_K U_{K|2K-1} \tag{19}$$

where the future state, $X_f = X_K = [x[K], x[K+1], \cdots, x[K+N-1]] \in \mathbb{R}^{n\times N}$, defines the past and future output and input information matrices

$$\begin{aligned} W_p &\triangleq \begin{bmatrix} U_p \\ Y_p \end{bmatrix} = \begin{bmatrix} U_{0|K-1} \\ Y_{0|K-1} \end{bmatrix}, \\ W_f &\triangleq \begin{bmatrix} U_f \\ Y_f \end{bmatrix} = \begin{bmatrix} U_{K|2K-1} \\ Y_{K|2K-1} \end{bmatrix}. \end{aligned}$$

Following the methodology presented in [18], [20], [21], the state matrix, X_f, serves as a memory for exchanging between past and future information. It is a basis for the intersection of past and future subspaces and can be computed using the SVD technique as outlined below, due to the fact that SVD does not produce a single, unique solution. The following formulation is one of the possible implementations.

The projection of Y_f onto W_p along U_f is

$$\xi = \hat{E}_{\|U_f}\left\{Y_f \mid W_p\right\}, \tag{20}$$

and the SVD of ξ is

$$\xi = \begin{bmatrix} U_1 & U_2 \end{bmatrix} \begin{bmatrix} \Sigma_1 & 0 \\ 0 & 0 \end{bmatrix} \begin{bmatrix} V_1^{\mathrm{T}} \\ V_2^{\mathrm{T}} \end{bmatrix} = U_1 \Sigma_1 V_1^{\mathrm{T}} \tag{21}$$

Then we have

$$\begin{aligned} \xi &= \mathcal{O}_K X_f \in \mathbb{R}^{Kp\times N} \\ \mathcal{O}_K &= U_1 \Sigma_1^{1/2} T \in \mathbb{R}^{Kp\times n}, \quad |T| \neq 0 \\ X_f &= T^{-1} \Sigma_1^{1/2} V_1^{\mathrm{T}} \in \mathbb{R}^{n\times N}. \end{aligned}$$

where $n = \dim \Sigma_1$ and $T \in \mathbb{R}^{n\times n}$ is an arbitrary nonsingular matrix.

B. Derivation of Linear State-Space Equation

In the preceding section, we acquired the state estimation, X_K. We introduce the subsequent matrices, each with $N-1$ columns, as defined below:

$$\begin{aligned} \bar{X}_{K+1} &\triangleq \begin{bmatrix} x[K+1] & \cdots & x[K+N-1] \end{bmatrix} \\ \bar{X}_K &\triangleq \begin{bmatrix} x[K] & \cdots & x[K+N-2] \end{bmatrix} \\ \bar{U}_{K|K} &\triangleq \begin{bmatrix} u[K] & \cdots & u[K+N-2] \end{bmatrix} \\ \bar{Y}_{K|K} &\triangleq \begin{bmatrix} y[K] & \cdots & y[K+N-2] \end{bmatrix}. \end{aligned} \tag{22}$$

The state-space model can then be derived using least squares in the subspace identification method while imposing the causality condition of $\underline{D}$ [17].

$$\begin{aligned} \begin{bmatrix} \hat{A} & \hat{B} \\ \hat{C} & \hat{D} \end{bmatrix} = &\left(\begin{bmatrix} \bar{X}_{K+1} \\ \bar{Y}_{K|K} \end{bmatrix} \begin{bmatrix} \bar{X}_K \\ \bar{U}_{K|K} \end{bmatrix}^{\mathrm{T}} \right) \\ &\cdot \left(\begin{bmatrix} \bar{X}_K \\ \bar{U}_{K|K} \end{bmatrix} \begin{bmatrix} \bar{X}_K \\ \bar{U}_{K|K} \end{bmatrix}^{\mathrm{T}} \right)^{-1} \end{aligned} \tag{23}$$

The state-space realization derived from the Hankel matrix [22] may also be applied in this context, where the parameters $(\underline{A}, \underline{B}, \underline{C}, \underline{D})$ are determined through the examination of the extended observability and controllability matrices. This alternative approach potentially offers enhanced robustness in the model's formulation.

IV. Derivation of the Fast Single-Rate Model

In this section, we formulate the fast single-rate model using the lifted mixed-rate model. Given the lifted state space, $(\underline{A}, \underline{B}, \underline{C}, \underline{D})$, the initial step discretizes the lifted state space with a period of mT, denoted as (A_{mT}, B_{mT}, C, D). Subsequently, we aim to recover the state space (A, B, C, D).

From the given data, the matrices $\underline{B}$ and $\underline{C}$ is expressed as

$$\begin{aligned} \underline{B} &= \begin{bmatrix} B_1 & B_2 & \cdots & B_n \end{bmatrix}, \\ \underline{C} &= \begin{bmatrix} C_1^T & C_2^T & \cdots & C_m^T \end{bmatrix}^T. \end{aligned} \tag{24}$$

It is evident that $B_{mT} = B_n = \sum_{i=0}^{m-1} A^i B$, $C = C_1$, and $D = 0$, the latter meeting the causality condition [17].

Assuming that the matrix $\underline{A}$ is diagonalizable, a premise for subspace system identification algorithm as elaborated in subsequent sections of [17] show that

$$P^{-1} \underline{A} P = \operatorname{diag}\left(\underline{\lambda}_1, \underline{\lambda}_2, \cdots, \underline{\lambda}_p\right),$$

wherein the columns of P embody the eigenvectors, and the elements $\underline{\lambda}_1, \underline{\lambda}_2, \cdots, \underline{\lambda}_p$ represent the corresponding eigenvalues of $\underline{A}$. Assuming $\underline{A} = A^{mn_1n_2}$ implies that A and $\underline{A}$ possess identical eigenvectors. If $\rho_i = \alpha_i + j\beta_i$ identifies as a pole of the system G, then the following relationship is established:

$$\lambda_i = e^{mn_1n_2T_s\rho_i} = e^{mn_1n_2T_s\alpha_i} \mathrm{e}^{jmn_1n_2\beta_i}.$$

The eigenvalues of A, denoted as λ_i for $i = 0, 1, \ldots, p-1$, facilitate the computation of matrix A. Application of P^{-1} to the final two columns of $\underline{B}$, specifically B_{n-1} and B_{n-2}, yields two vector columns

$$P^{-1}B_{n-1} = \begin{bmatrix} a_0 \\ a_1 \\ \vdots \\ a_{p-1} \end{bmatrix}, \quad P^{-1}B_{n-2} = \begin{bmatrix} b_0 \\ b_1 \\ \vdots \\ b_{p-1} \end{bmatrix}.$$

Given $B_{n-2} = A_{mT} B_{n-1}$, the eigenvalues λ_i are ascertainable from the component ratios in the vectors as

$$\lambda_i = \frac{b_i}{a_i}, \quad \text{for } i = 0, 1, \ldots, p-1.$$

Then the reconstruction of the matrix A is

$$A = P \operatorname{diag}\left\{\lambda_0, \lambda_1, \ldots, \lambda_{p-1}\right\} P^{-1}$$

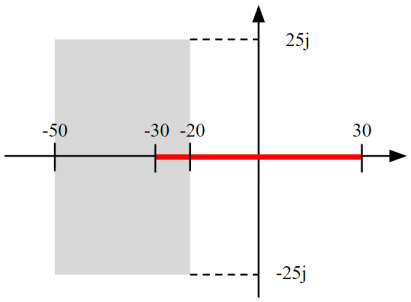

Fig. 4. Graphical representation of the pole-zero configuration within the complex plane. Poles (shaded gray region) were positioned away from the origin for rapid transient demonstration, with system identification prioritizing steady-state responses. The remaining six poles' real parts range from -20 to -50, with imaginary parts from -25 to 25. Zeros' (red line) real parts are randomly set between -30 to 30.

V. Numerical Illustration

We illustrate the underlying principles of the multirate system with an 8^{th} order plant. More specifically, we arbitrarily generated four zeros and six poles, along with the placement of a pair complex-conjugate poles within the specified gray area in Fig. 4.

The plant under such consideration can be mathematically represented as:

$$G(s) = \frac{\sum_{i=0}^{4} a_i s^{4-i}}{\sum_{i=0}^{8} b_i s^{8-i}} \tag{25}$$

Despite its random generation, the system is bounded-input, bounded-output (BIBO) stable for proper system identification with the designed region of stable poles[1].

The computational simulation was executed using MATLAB Simulink operating at a frequency of $F_s = 1024$ Hz. The chosen input mechanism was a zero-order hold, which was maintained for a control duration equivalent to $2T$. In this setup, two distinct sensors were integrated, characterized by unique coprime frequencies. Specifically, the two sensors operated at a frequency $3\times$ and $5\times$ slower than the system sampling period, respectively. This is denoted as $m = 2$, $n_1 = 3$, and $n_2 = 5$. The Nyquist sampling frequency is $F_s/(2n_1)$ for the first sensor and $F_s/(2n_2)$ for the second sensor.

Fig. 6 illustrates a comparative analysis of the frequency responses between the actual system and the inferred system models. It's imperative to highlight the observed congruence between the estimated system's frequency response and that of the genuine system. This congruence signifies the efficacy of the estimation technique, emphasizing its proficiency in accurately delineating the inherent dynamics and attributes of the real system. Fig. 5 shows the limitation of a singular sensor in capturing peaks surpassing its Nyquist sampling frequency. However, our novel collaborative sensing methodology ensures that system dynamics are effectively approximated beyond each individual sensor's Nyquist sampling frequency. Such an observation emphasizes the value and efficacy of integrating multiple sensors for enhanced system identification performance as opposed to relying on a singular sensor.

[1]For unstable plants, closed-loop system identification can be performed after stabilizing the plants.

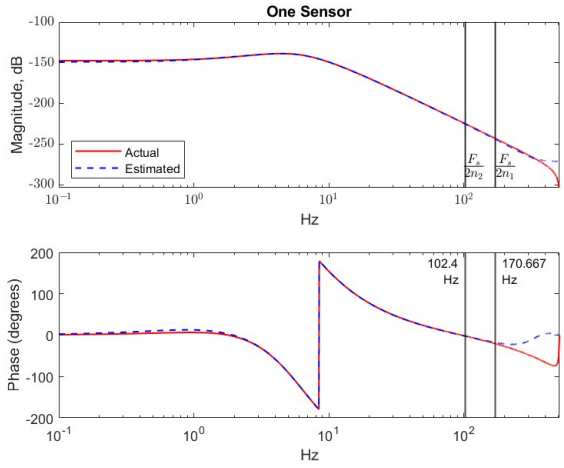

Fig. 5. In this setup, a single sensor is insufficient for accurately capturing the system dynamics, highlighting the need for cooperative sensing

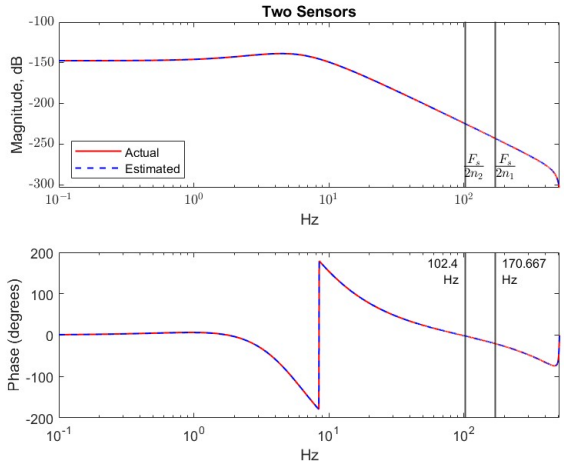

Fig. 6. Efficiency of a Dual-Sensor System: This illustration showcases the system's stable output achieved by the operation of two sensors with coprime sampling periods, guaranteeing a robust capture of system dynamics

In addition to the preceding analysis, the algorithm's performance was evaluated on an 8^{th} order non-minimum phase (NMP) system as shown in Figs. 7 and 8. This system exhibits two zeros in the right half-plane and two in the left half-plane. The analysis highlights the single-sensor's inadequacy in accurately representing the dynamics of a NMP system, with its inability to capture the system's dynamic behavior effectively. In contrast, a dual-sensor configuration substantially improves the precision and dependability of dynamic system capture, providing a robust and thorough insight into the NMP system's behavior. Experimental and analytical evidence confirms the two-sensor system's improved capabilities in identifying the complexities of NMP

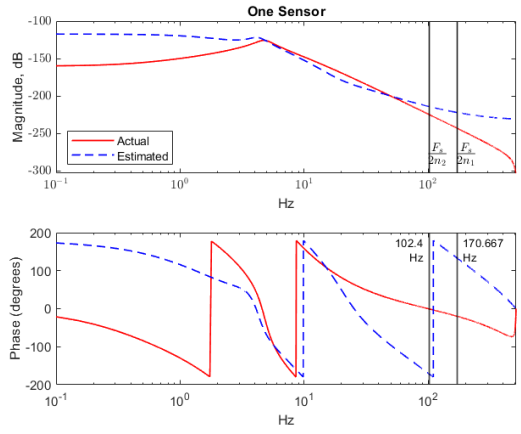

Fig. 7. In the context of a non-minimum phase system setup, a single sensor proves inadequate for capturing the complete system dynamics accurately.

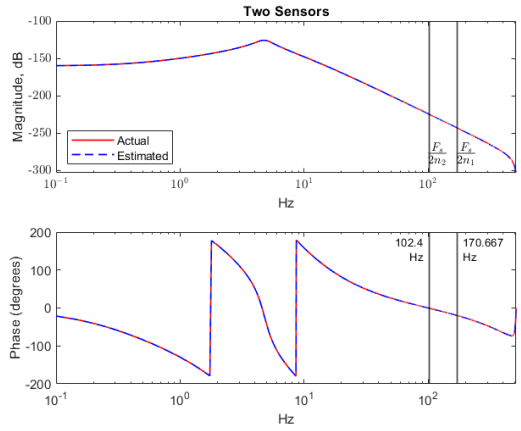

Fig. 8. Contrastingly, a Dual Sensor System adeptly encapsulates the intricate dynamics of the non-minimum phase system, ensuring a precise capture of system behavior.

systems.

VI. Conclusion and Future Work

This research proposes a pioneering methodology to model multirate sampled-data systems using lifted state-space representation. By leveraging non-uniform data derived from the coprime collaborative sensing mechanism, our framework can identify system dynamics beyond the Nyquist frequency of the single-rate sensor. Our method's empirical validation across minimum phase and NMP systems shows its robustness and broad applicability. Advancing further, it is imperative to incorporate filtering techniques to enhance intersample estimates and facilitate recursive system identification. There is promising work in utilizing features from Hankel matrices to develop data-driven control strategies, which circumvent the need for an explicit realization process and instead directly utilize the state vector for implementing closed-loop control [23] [24].

References

[1] R. D. Gudi, S. L. Shah, and M. R. Gray, "Multirate state and parameter estimation in an antibiotic fermentation with delayed measurements," *Biotechnology and Bioengineering*, vol. 44, no. 11, pp. 1271–1278, 1994.

[2] M. Li, H. McAllister, and N. Black, "Multirate modeling of human ear frequency resolution for hearing aids," in *1996 IEEE Digital Signal Processing Workshop Proceedings*, 1996, pp. 157–160.

[3] R. E. Crochiere and L. R. Rabiner, *Multirate digital signal processing*. Prentice-hall Englewood Cliffs, NJ, 1983, vol. 18.

[4] J. Berg, K.-Y. Ting, T. J. Mundt, M. Mor, E. Livne, and K. A. Morgansen, "Exploratory wind tunnel gust alleviation tests of a multiple-flap flexible wing," in *AIAA SCITECH 2022 Forum*, ser. AIAA SciTech Forum. American Institute of Aeronautics and Astronautics, 2021.

[5] D. Wang and X. Chen, "A multirate repetitive control for fractional-order servos in laser-based additive manufacturing," in *2018 Annual American Control Conference (ACC)*, 2018, pp. 4831–4836.

[6] Y. Wu and G. Chiu, "An improved height difference based model of height profile for drop-on-demand 3d printing with uv curable ink," in *2021 American Control Conference (ACC)*, 2021, pp. 491–495.

[7] D. Wang and X. Chen, "A multirate fractional-order repetitive control for laser-based additive manufacturing," *Control Engineering Practice*, vol. 77, pp. 41–51, 2018.

[8] M. Ohshima, I. Hashimoto, H. Ohno, M. Takeda, T. Yoneyama, and F. Gotoh, "Multirate multivariable model predictive control and its application to a polymerization reactor," *International Journal of Control*, vol. 59, no. 3, pp. 731–742, 1994.

[9] G. Kranc, "Input-output analysis of multirate feedback systems," *IRE Transactions on Automatic Control*, vol. 3, no. 1, pp. 21–28, 1957.

[10] F. Ding and T. Chen, "Least squares based self-tuning control of dual-rate systems," *International Journal of Adaptive Control and Signal Processing*, vol. 18, no. 8, pp. 697–714, 2004.

[11] W. Yan, C. Du, and C. K. Pang, "A general multirate approach for direct closed-loop identification to the nyquist frequency and beyond," *Automatica*, vol. 53, pp. 164–170, 2015.

[12] G. C. Goodwin and K. S. Sin, *Adaptive Filtering Prediction and Control*. USA: Dover Publications, Inc., 2009.

[13] L. Ljung, *System Identification: Theory for the User*, ser. Prentice Hall Information and System Sciences Series. Prentice Hall PTR, 1999.

[14] J. Ouyang and X. Chen, "Least squares solution for system identification with non-uniform data under a coprime collaborative sensing scheme," in *2023 American Control Conference (ACC)*, 2023, pp. 1570–1575.

[15] P. P. Vaidyanathan and P. Pal, "Sparse sensing with coprime arrays," in *2010 Conference Record of the Forty Fourth Asilomar Conference on Signals, Systems and Computers*, 2010, pp. 1405–1409.

[16] T. Chen and B. A. Francis, *Optimal Sampled-Data Control Systems*. Springer Science & Business Media, 2012.

[17] D. Li, S. L. Shah, and T. Chen, "Identification of fast-rate models from multirate data," *International Journal of Control*, vol. 74, no. 7, pp. 680–689, 2001.

[18] M. Viberg, "Subspace-based methods for the identification of linear time-invariant systems," *Automatica*, vol. 31, no. 12, pp. 1835–1851, 1995, trends in System Identification.

[19] A. Tether, "Construction of minimal linear state-variable models from finite input-output data," *IEEE Transactions on Automatic Control*, vol. 15, no. 4, pp. 427–436, 1970.

[20] M. Moonen, B. De Moor, L. Vandenberghe, and J. Vandewalle, "On- and off-line identification of linear state-space models," *International Journal of Control*, vol. 49, no. 1, pp. 219–232, 1989.

[21] T. Katayama, *Subspace methods for system identification*. Springer, 2005, vol. 1.

[22] W. Gray, E. Verriest, and F. Lewis, "A hankel matrix approach to singular system realization theory," in *29th IEEE Conference on Decision and Control*, 1990, pp. 73–78 vol.1.

[23] H. J. van Waarde, J. Eising, H. L. Trentelman, and M. K. Camlibel, "Data informativity: a new perspective on data-driven analysis and control," 2019.

[24] C. De Persis and P. Tesi, "Formulas for data-driven control: Stabilization, optimality, and robustness," *IEEE Transactions on Automatic Control*, vol. 65, no. 3, pp. 909–924, 2020.